CHEMICAL EVOLUTION OF THE GALACTIC DISK WITH RADIAL GAS FLOWS

CEDRIC G. LACEY[1,2] AND S. MICHAEL FALL[1,3]

ABSTRACT

We present a series of models for the chemical evolution of the galactic disk with radial inflows of the gas at a velocity that is constant in time but may vary with galactocentric radius. The models also include the infall of metal-free gas from outside the disk at a rate that decays exponentially with time, a star formation rate that varies as the *m*th power of the surface density of the gas layer, with $m = 1$ or 2, and in some cases an outer edge to the stellar disk at a radius r_*. Chemical evolution is treated in the approximation of instantaneous recycling, with a constant initial mass function. The models are compared with the observed age-metallicity relation and metallicity distribution for stars in the solar neighborhood and with the observed radial variations of the metallicity, the star formation rate, and the surface densities of gas and stars. We find that all of the observational data can be fitted when radial flows at velocities $v_r \approx -(0.5-1.0)$ km s^{-1} are included in the models. Inflow velocities of this order of magnitude are expected on theoretical grounds and are consistent with the available observations. For models with $m = 1$, the interaction between inflows and a star formation edge, taken to be at $r_* \approx 18$ kpc, is important for producing metallicity gradients. For models with $m = 2$, the metallicity gradient mainly results from the density-dependence of the star formation efficiency. Infall is still needed to give agreement with the observations in the solar neighborhood, the present total infall rates for acceptable models being in the range $\dot{M}_D \approx (0.1 - 1)$ $M_\odot$ yr^{-1}, with larger values for $m = 1$ than for $m = 2$.

Subject headings: galaxies: evolution — galaxies: internal motions — galaxies: Milky Way — galaxies: stellar content

I. INTRODUCTION

As part of a previous investigation, we computed a series of models for the chemical evolution of the galactic disk and compared them with a variety of observational constraints (Lacey and Fall 1983, hereafter Paper I). In these models, infall of metal-free gas was assumed to occur at a rate that decayed exponentially on a time scale t_f and stars were assumed to form with a constant initial mass function at a rate proportional to the *n*th power of the volume density of the gas layer. Chemical enrichment was treated in the approximation of instantaneous recycling, with no exchange of material between different galactocentric radii. We found that models with $n = 1$ and $t_f = 6$ Gyr or $n = 2$ and $t_f = 2$ Gyr were compatible with the age-metallicity relation and the metallicity distribution for stars in the solar neighborhood. The $n = 1$ models also reproduced the observed radial variations in the gas density and star formation rate. However, none of the models had an acceptable metallicity gradient, even when the input parameters governing infall and star formation were allowed to vary with galactocentric radius.

Several mechanisms have been proposed to explain chemical abundance gradients in galactic disks. One possibility is that the initial mass function (IMF) of the stars varies with position such that relatively more high-mass stars are produced at smaller galactocentric radii (e.g., Quirk and Tinsley 1973; Güsten and Mezger 1982). Garmany, Conti, and Chiosi (1982) have presented evidence, based on counts of early-type stars in our Galaxy, for spatial variations in the upper IMF in just this sense. However, Humphreys and McElroy (1984) attribute this result to selection effects and claim that the data actually favor

a constant IMF. Temporal variations in the IMF were first proposed as one possible solution of the G dwarf problem in the solar neighborhood (Schmidt 1963). They have also been invoked to explain differences in the relative abundances of elements in stars with different ages (Clegg, Lambert, and Tomkin 1981 and references therein), although Twarog and Wheeler (1982) argue that variations in the IMF are not required in the galactic disk. On physical grounds, it would be surprising if the IMF were exactly constant, but this simplifying assumption may be reasonable as a first approximation.

Another mechanism for producing or enhancing chemical abundance gradients, which was proposed by Tinsley and Larson (1978), is radial gas flows within the galactic disk. The only models to date that include such flows are those of Mayor and Vigroux (1981). They considered the particular case of inflow driven by the infall of gas with zero angular momentum but did not make use of the observations relating to the chemical evolution of the solar neighborhood in constraining their models. Radial flows might also be driven by viscosity in the gas layer or by gravitational interaction with a density wave in the stellar disk. Present observational limits are consistent with flow velocities of up to a few km s^{-1}. In this paper we investigate in more generality the effects of radial inflows, combined with infall, on the chemical evolution of the galactic disk when the IMF is assumed to be constant.

The plan for the remainder of the paper is as follows. In § II, we discuss the main ingredients of the models and the equations used. These are similar to the models in Paper I except for the inclusion of radial gas flows and the assumption that the star formation rate varies as a power *m* of the surface density of the gas. The observations to be used as input parameters and as constraints on the models are reviewed in § III. Some of the data are the same as in Paper I, but there have been enough improvements, particularly regarding the gas density, to

[1] Institute of Astronomy, University of Cambridge.
[2] Department of Astrophysical Sciences, Princeton University.
[3] Institute for Theoretical Physics, University of California.

154

warrant another discussion here. In § IV, we present the results of the models and discuss the interactions between inflow, infall, and the efficiency of star formation. We find that radial flows are particularly effective at producing a metallicity gradient when star formation is suppressed at large galactocentric radii. Finally, our main conclusions are listed in § V.

II. BASIC ASSUMPTIONS AND EQUATIONS

a) Chemical Evolution

We compute the surface densities μ_g and μ_s of gas and stars and the abundance Z of primary elements in the gas as functions of radius r and time t. These quantities evolve due to the formation of new stars, the ejection of matter by evolved stars, the infall of metal-free gas from outside the disk, and the radial flow of the gas already in the disk. We neglect any secular variations in the gravitational field of the Galaxy arising from radial flows and infall, since a large part of this field is produced by the spheroid and the dark halo. Thus, the stars are treated as being fixed in radius and the radial velocity v_r of the gas is equal to its velocity relative to the stars. We also assume that the IMF is constant and treat the ejection of matter by evolved stars in the approximation of instantaneous recycling. Defining ψ and f to be, respectively, the azimuthally averaged star formation rate and infall rate per unit area, the standard equations governing the chemical evolution of the galactic disk are

$$\frac{\partial \mu_s}{\partial t} = (1 - R)\psi , \qquad (1)$$

$$\frac{\partial \mu_g}{\partial t} = -(1 - R)\psi + f - \frac{1}{r} \frac{\partial}{\partial r} (r v_r \mu_g) , \qquad (2)$$

and

$$\mu_g \frac{\partial Z}{\partial t} = y(1 - R)\psi - fZ - \mu_g v_r \frac{\partial Z}{\partial r} \qquad (3)$$

(e.g., Tinsley 1980). The returned fraction R and the yield of primary elements y need not be specified at the outset since they enter the equations only through the combinations $(1 - R)\psi$ and Z/y. If the metallicity of the infalling gas is nonzero, with a value Z_f, a term fZ_f must be added to the right-hand side of equation (3), but for $Z_f \lesssim 0.1 Z_\odot$ this will have little effect on the chemical evolution. We have also computed the evolution of the abundance of secondary elements, and mention the results briefly in § IVa. In the remainder of this section, we discuss the functional forms assumed for f, ψ, and v_r.

b) Infall Rate

Infall was originally introduced into chemical evolution models as one possible solution of the G dwarf problem in the solar neighborhood (Larson 1972; Lynden-Bell 1975). It may also be desirable in order to prevent the complete consumption of gas in spiral galaxies on time scales shorter than their ages and may be a natural consequence of galaxy formation from extended halos (Larson, Tinsley, and Caldwell 1980; Kennicutt 1983). The infall rate $f(r, t)$ is difficult to predict in detail because it depends on the way the Galaxy formed and on the dynamics of the gaseous halo; the accreted material could be in the form of diffuse gas, discrete clouds, or dwarf galaxies. Therefore we adopt the same parameterization as in Paper I, in which the infall rate decays exponentially with radius and time:

$$f(r, t) = \frac{\alpha_f^2 M_D(t_1)}{2\pi} \frac{\exp(-\alpha_f r - t/\tau)}{\tau[1 - \exp(-t_1/\tau)]} , \qquad (4)$$

where $M_D(t_1)$ is the total mass of the disk at the present time, $t = t_1$. The radial dependence is chosen because we want the models to have roughly exponential surface density profiles, although radial flows will modify this. The time dependence is chosen because it is physically reasonable and mathematically convenient. For reference, we note that the free-fall time from a radius of 100 kpc in an isothermal halo with a circular velocity of 220 km s^{-1} is about 0.6 Gyr. We have also computed several models without infall, designated $\tau = 0$, in which the initial gas density was taken to be $\mu_g(r, 0) = [\alpha_f^2 M_D(t_1)/2\pi] \exp(-\alpha_f r)$.

c) Star Formation Rate

Here we assume that the star formation rate varies as a power m of the surface density of the gas:

$$(1 - R)\psi = C\mu_g{}^m , \qquad (5)$$

where C is a constant. In Paper I we followed Schmidt's (1959) prescription and assumed that the star formation rate varied as a power n of the volume density of the gas. However, this form required calculation of the scale height of the gas layer, which in turn required assumptions about the pressure support in the vertical direction. Equation (5) is a reasonable simplification since the volume density form has only a rough empirical justification, and the surface density form serves equally well for investigating the way in which the star formation rate affects metallicity gradients when radial flows are present. The two forms are equivalent for $m = n = 1$ whatever the scale height of the gas layer, and are also equivalent for any values of m and n when the scale height is constant with galactocentric radius.

In some of the models, star formation is suppressed at large radii. The main motivation for including this effect is that the stellar disks of many galaxies are observed to have outer edges at radii r_{max} about equal to their Holmberg radii, whereas the gas layers usually extend beyond this (van der Kruit and Searle 1982; Sancisi 1983). Presumably the cutoff results from a lower efficiency of star formation in the outer parts of the disks where the density of the gas is low. Fall and Efstathiou (1980) have suggested that star formation begins at a given radius only if the gas layer is gravitationally unstable according to the condition derived by Goldreich and Lynden-Bell (1965). For an isothermal gas layer that is self-gravitating in the vertical direction, we have

$$G\mu_g/\sigma_g \kappa > 0.27 , \qquad (6)$$

where κ is the epicyclic frequency and σ_g is the three-dimensional velocity dispersion of the gas. Depending on the assumed value of σ_g, this condition predicts values of r_{max} in rough agreement with the observations. Thus it is plausible that the gravitational instability condition (6), or some modification of it, is responsible for the edges in stellar disks. In this paper, we take a simpler approach to including star formation edges in the models: ψ is given by equation (5) for $r < r_*$ and $\psi = 0$ for $r > r_*$, where r_* is fixed by observations. Clearly this approach bypasses all questions about the physical mechanism and ignores the possible time dependence of r_{max}, but it should be adequate to illustrate the importance of an edge for the chemical evolution of the disk when radial flows are included.

d) Radial Gas Flows

Several mechanisms could drive a radial gas flow in the galactic disk, although the details are highly uncertain. The first possibility is that the specific angular momentum of the infalling gas h_f differs from the value h_c for circular motions in the disk. In this case, mixing will induce a radial velocity

$$v_r \approx -\frac{f}{\mu_g}\frac{(h_c - h_f)}{dh_c/dr} \qquad (7)$$

for $|v_r| \ll h_c/r$. Mayor and Vigroux (1981) considered the effects of such a flow on chemical evolution for the special case $h_f = 0$. However, the Galaxy may still be accreting from an envelope of gas left over from its formation, in which case the infalling material would presumably have some angular momentum and the radial inflow in the disk would be correspondingly reduced. Unfortunately, $h_f(r, t)$, like $f(r, t)$, cannot be predicted in detail without a specific model for the gaseous halo of the Galaxy. To estimate the order of magnitude of the flows that might be expected, we take $h_f = 0$, $f = 1$ $M_\odot$ pc^{-2} Gyr^{-1}, $\mu_g = 10$ $M_\odot$ pc^{-2}, and a flat rotation curve, and find $v_r \approx -1$ km s^{-1} at $r \approx 10$ kpc.

The second possible mechanism for driving radial flows is viscosity in the gas layer. An effective viscosity ν would induce a velocity $|v_r| \sim \nu/r$ at a radius r, the flow being inward in the inner parts of the Galaxy and outward in the outer parts (Lynden-Bell and Pringle 1974). For a fluid of particles with mean free path l, total velocity dispersion σ, and epicyclic frequency κ, the kinematic viscosity is

$$\nu \approx \frac{\sigma^3 l}{3[(\kappa l)^2 + \sigma^2]} \qquad (8)$$

(Goldreich and Tremaine 1978; Fukunaga 1983). This expression is valid whether the particles are gas atoms or gas clouds, but the viscosity due to atomic collisions is negligible in comparison with the viscosity due to cloud collisions. For H I clouds, with $l \approx 300$ pc and $\sigma \approx 14$ km s^{-1}, we estimate $\nu \approx 1$ km s^{-1} kpc. For the giant molecular clouds, with $\sigma \approx 6$ km s^{-1}, the gravitational interactions must be included in calculating the collision rates. By a method analogous to that of Chandrasekhar (1960), but treating the system as two dimensional, we find a mean free path for the giant molecular clouds of $l \sim 300$ pc and thus $\nu \sim 0.1$ km s^{-1} kpc. Adding the viscosities of the two components in proportion to their surface densities, we estimate a radial velocity of $|v_r| \sim 0.1$ km s^{-1} at $r \approx 10$ kpc.

The third possible mechanism for driving radial flows is the gravitational interaction between the gas and a bar or spiral density wave in the stellar disk. As Kalnajs (1972) pointed out, even a steady wave will induce a net radial flow, averaged over azimuth, if the response of the gas involves dissipation, which is most likely to occur via large-scale shocks. Using his results, we derive the following relation between the flow velocity v_r and the rate of energy dissipation per unit radius $\dot{E}_d$:

$$v_r \approx \frac{\dot{E}_d}{2\pi r \mu_g(\Omega_p - \Omega_c)(d/dr)(\Omega_c r^2)}, \qquad (9)$$

where Ω_p and Ω_c are, respectively, the angular velocities of the wave pattern and of circular orbits (valid for $|v_r| \ll \Omega_c r$). Since the dissipation rate must always satisfy $\dot{E}_d \geq 0$, any gas flow will be inward inside corotation [$\Omega_c(r) > \Omega_p$] and outward outside corotation [$\Omega_c(r) < \Omega_p$]. A self-consistent calculation
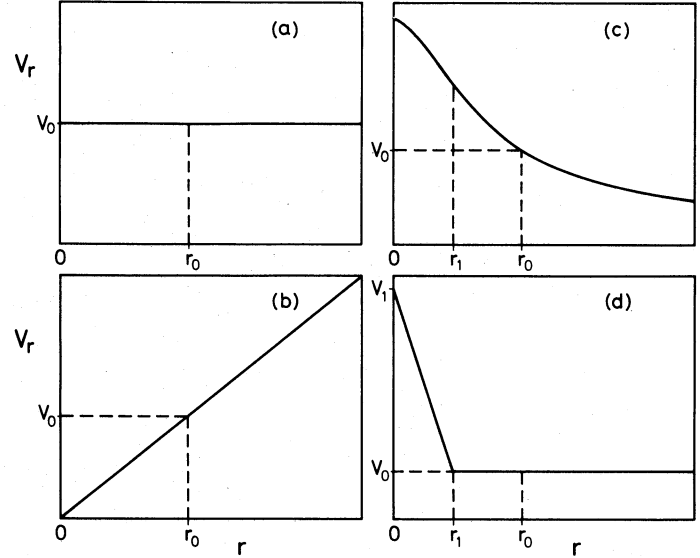

FIG. 1.—Model velocity fields for radial gas flows; v_r is given explicitly as a function of galactocentric radius in eqs. (10)–(13) of the text and is assumed to be constant in time.

of the gas response is required to predict $\dot{E}_d$ and thus v_r, which in turn depends on the form of the density wave and the physical state of the gas. Roberts, Shu, and co-workers have computed the response of an isothermal fluid to a tightly wound spiral potential that is intended to model the spiral structure in our Galaxy (e.g., Roberts 1969; Shu, Milione, and Roberts 1973). From their version of equation (9), Roberts and Shu (1972) derive a radial flow velocity of $v_r \approx -0.3$ km s^{-1} at $r \approx 10$ kpc. Fully two-dimensional, time-dependent calculations of the response of gas to barlike density waves have given much larger radial flow velocities (Schwarz 1981; van Albada and Roberts 1981 and references therein). However, it is not clear to what extent this is due to the larger non-axisymmetric forces involved, rather than to numerical viscosity in the calculations or to the method of treating cloud collisions. In a strongly barred galaxy, the radial excursions of the gas and stars may lead to mixing of the chemical composition at different radii. This effect, which is not included in the models, would tend to reduce the metallicity gradient rather than enhance it. In any case, the influence of a bar in our Galaxy, if one exists, is probably negligible beyond a few kpc from the center.

In conclusion, estimates based on various physical mechanisms suggest that radial velocities of order $|v_r| \sim (0.1-1)$ km s^{-1} may be expected, and further that these are likely to be inflows rather than outflows over the main body of the Galaxy. However, the variation of v_r with radius and time is completely uncertain theoretically, so our approach is to investigate the effects of various imposed functions $v_r(r, t)$. For simplicity, we take v_r to be constant in time and monotonic and single signed in radius, with one of four simple forms: constant, increasing, decreasing, or with a spike at the center; these are illustrated in Figure 1 and listed below:

(a) Constant:

$$v_r = v_0 . \qquad (10)$$

(b) Increasing:

$$v_r = v_0(r/r_0) . \qquad (11)$$

(c) Decreasing:

$$v_r = v_0\left(\frac{r_0^2 + r_1^2}{r^2 + r_1^2}\right)^{1/2}. \qquad (12)$$

(d) Central spike:

$$v_r = \begin{cases} v_1 + (v_0 - v_1)r/r_1 & r \le r_1 \\ v_0 & r \ge r_1 \end{cases}. \qquad (13)$$

In all cases, r_0 is the galactocentric radius of the Sun, v_0 is the corresponding radial velocity, and, in equations (12) and (13), the characteristic radius is taken to be $r_1 = 4$ kpc.

e) Integration of the Equations

For the purposes of numerical integration, equations (1)–(3) were cast into conservative form, using the variable $Z\mu_g$ instead of Z. We then used the Lelevier method (Potter 1973) to approximate the radial derivatives on a grid of equal spacing, and the second-order Runge-Kutta method to step forward in time, with equal increments. The initial conditions were taken to be $\mu_g(r, 0) = \mu_s(r, 0) = Z(r, 0) = 0$, except for the special case $\tau = 0$ mentioned in § IIb, and the equations were integrated from $t = 0$ to $t = t_1$. As an inner boundary condition, the gas was simply allowed to pile up in the central zone. Since the disk was assumed to have infinite radial extent, no outer boundary condition was in principle needed. In practice, however, the errors caused by the finite size of the grid could propagate inward and affect the solution in the radial range of interest. We dealt with this problem in some cases by joining on approximate analytic solutions at large radii, and in others by simply increasing the radial extent of the grid until increasing it further made no significant difference to the results. A typical model, with 100 time steps and 100 radial zones extending out to $r = 50$ kpc, required 20 s of CPU time on a VAX 11/780 and gave an accuracy of a few percent. The program was checked against simple analytical solutions for a variety of special cases.

III. OBSERVATIONAL INPUTS AND CONSTRAINTS

a) Structure of the Stellar Disk

The stellar disk of our Galaxy is assumed, by comparison with similar spirals, to have a surface density profile that is roughly exponential with a scale length of $\alpha_s^{-1} = (4 \pm 1)$ kpc (de Vaucouleurs and Pence 1978; Bahcall and Soneira 1980; van der Kruit 1983). This is based on an adopted galactocentric radius for the Sun of $r_0 = 8.5$ kpc, and all of the observational data to be compared with the models are scaled accordingly. There is some direct evidence for an outer cutoff in the stellar disk of our Galaxy. Chromey (1978) finds that the distribution of OB stars in the anticenter direction declines markedly beyond $r_{max} \approx 20$ kpc, while Fich and Blitz (1984) find that the distribution of H II regions ends beyond about $r_{max} \approx (16–20)$ kpc, depending on the adopted rotation curve. Indirect evidence on the radius of the cutoff comes from the observation that strong warping of the gas layer begins at $r \approx (15–17)$ kpc (Kulkarni, Blitz, and Heiles 1982; Henderson, Jackson, and Kerr 1982), and the near coincidence of this feature with the edges of the stellar disks in other galaxies (Sancisi 1983). In the models with a star formation cutoff, we therefore adopt $r_* = 18$ kpc, which is consistent with the relation $\alpha_s r_{max} = 4.7 \pm 0.7$ derived from van der Kruit and Searle's (1982) photometry of nearby spiral galaxies.

The stellar disk of our Galaxy might also have deviations from exponential behavior at small radii. Kormendy (1977)

finds evidence for central holes of radius $r \sim \alpha_s^{-1}$ in other galaxies, and a central hole of radius $r \approx 2$ kpc was included in Caldwell and Ostriker's (1981) mass model of our Galaxy. Closer to the center, there may be a very significant excess of mass: Oort's (1977) study and the galactic mass models of Caldwell and Ostriker (1981) and Bahcall, Schmidt, and Soneira (1983) all give a total mass within 1 kpc of about $1.5 \times 10^{10} M_\odot$. Since part or all of this mass may be associated with the spheroid, we interpret it as an upper limit on any concentration in the disk.

Estimates of the total surface density of the disk in the solar neighborhood from the vertical force law give $(70 \pm 20) M_\odot$ pc^{-2} (Bahcall 1984, and references therein). Since the gas accounts for about 10 $M_\odot$ pc^{-2} (see next section), the local surface density of the stellar disk should be $\mu_s(r_0, t_1) \approx (60 \pm 20) M_\odot$ pc^{-2}. Combining these estimates with the adopted exponential scale length implies a present total disk mass of $M_D(t_1) \approx (6 \pm 2) \times 10^{10} M_\odot$. In principle, $M_D(t_1)$ could be treated as an adjustable parameter in the models, but in practice we find it convenient to compute all of the models with the same value of $M_D(t_1) = 6 \times 10^{10} M_\odot$. The observations and their uncertainties discussed above are then used to set constraints on the models; the surface density of stars should lie within the stippled region of Figure 3e, which allows for an outer cutoff, an inner hole, and a central mass concentration in the disk.

b) Surface Density of the Gas Layer

To estimate the total surface density of the gas in the galactic disk, we must add the contributions from the atomic hydrogen (H I), molecular hydrogen (H$_2$) and the associated helium. Figure 2 shows several determinations of the azimuthally averaged surface densities of H I and H$_2$ as functions of galactocentric radius. For the H I inside the solar circle, the largest systematic uncertainty arises from the optical depth of the 21 cm emission. The curve labeled BG, which is obtained from Burton and Gordon's (1978) volume densities and Baker and Burton's (1975) scale heights, is now thought to be too low because of underestimation of the optical depth, and a value $\mu_{HI} \approx (4–6) M_\odot$ pc^{-2} for $4 \lesssim r \lesssim 8.5$ kpc seems more realistic. This estimate is consistent with Heiles's (1976) determination of 6 $M_\odot$ pc^{-2} for the surface density of H I within about 1 kpc of the Sun. For the H I outside the solar circle, the largest systematic uncertainty results from the adoption of different rotation curves. There are two determinations, based in large part on the same observational data: that of Kulkarni, Blitz, and Heiles (1982) (KBH) assumes a slowly rising rotation curve, while that of Henderson, Jackson, and Kerr (1982) (HJK) assumes a flat rotation curve.

The surface density of H$_2$ is inferred from measurements of the z-integrated CO emissivity, I_{CO}, using a conversion factor $X \equiv N_{H_2}/I_{CO}$ which is usually assumed to be approximately independent of position in the disk. Three different methods have been used to estimate X. The first is based on measurements of the extinction of stars behind nearby molecular clouds; from the data of Dickman (1978) and Frerking, Langer, and Wilson (1982), Thaddeus (1983) derives $X \approx (1.5–2.0) \times 10^{20}$ cm^{-2} K^{-1} km^{-1} s, while Sanders, Solomon, and Scoville (1984), using ^{13}CO emission in an intermediate step, derive $X \approx 4 \times 10^{20}$ cm^{-2} K^{-1} km^{-1} s. The second method uses γ-ray counts to estimate hydrogen column densities: Lebrun et al. (1983) find $X \approx (1–3) \times 10^{20}$ cm^{-2} K^{-1} km^{-1} s for the galactic plane, while Hermsen and Bloemen (1984) find
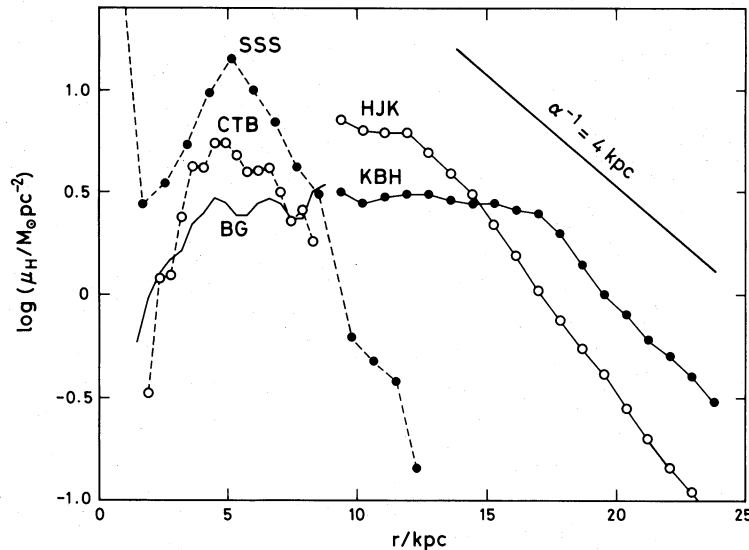
FIG. 2.—Observational determinations of the surface density of hydrogen gas as a function of radius. *(full curves)*: H I. *(dashed curves)*: H_2, using a CO-to-H_2 conversion factor $X = 3 \times 10^{20}$ cm^{-2} K^{-1} km^{-1} s. The labeling of the curves is as follows: BG: Burton and Gordon (1978) (using scale-height determination from Baker and Burton 1975); KBH: Kulkarni, Blitz, and Heiles (1982) (curve taken from Fig. 7 of Blitz, Fich, and Kulkarni 1983); HJK: Henderson, Jackson, and Kerr (1982) (average of north and south); SSS: Sanders, Solomon, and Scoville (1984); CTB: Cohen, Thaddeus, and Bronfman (1984).

$X \approx 3 \times 10^{20}$ cm^{-2} K^{-1} km^{-1} s for the nearby Orion complex. The third method is to estimate the masses of molecular clouds from the virial theorem: in this way, Sanders *et al.* infer $X \approx 5 \times 10^{20}$ cm^{-2} K^{-1} km^{-1} s. As a compromise between all three methods, we adopt $X = (3 \pm 1) \times 10^{20}$ cm^{-2} K^{-1} km^{-1} s for converting the CO emissivity data of Sanders *et al.* (SSS) and Cohen, Thaddeus, and Bronfman (1984) (CTB) into H_2 surface densities. Both sets of data are based on averages of the midplane emissivities for north and south and the scale heights determined for the north. As Figure 2 shows, there is a factor of 2 discrepancy arising from uncertainties in the CO emissivity alone.

To give a fair representation of all the uncertainties in the distribution of gas, we proceed as follows. Inside the solar circle, the minimum H I curve is taken to be that of Burton and Gordon (1978), while the maximum is taken to be twice this, to allow for reasonable optical depths. Outside the solar circle, we consider the Kulkarni *et al.* and Henderson *et al.* curves as upper and lower limits at each radius. The minimum H_2 is derived from the Cohen *et al.* emissivity with a conversion factor $X = 2 \times 10^{20}$ cm^{-2} K^{-1} km^{-1} s, while the maximum is derived from the Sanders *et al.* emissivity with $X = 4 \times 10^{20}$ cm^{-2} K^{-1} km^{-1} s. Adding the H I and H_2 together, multiplying by 4/3 to account for helium, and smoothing, we arrive at the limits represented by the stippled region of Figure 3*f*. The surface density profile derived in this way is approximately exponential with a scale length of 5 ± 1 kpc over the range 5 kpc $\lesssim r \lesssim$ 20 kpc and has a large deficiency over the range 1 kpc $\lesssim r \lesssim$ 5 kpc.

c) *Variations in the Abundance of Heavy Elements*

Detailed information on the history of chemical enrichment is only available for the solar neighborhood. Twarog (1980) obtained Strömgren indices for more than a thousand F dwarfs and derived a relation between mean metallicity and age using Ciardullo and Demarque's (1977) isochrones. Recently, Carlberg *et al.* (1984) have reanalyzed a subset of Twarog's data using Vandenberg's (1983) isochrones. Their relation is signifi-

cantly flatter than Twarog's as a result of a 20%–40% difference in the ages derived from the two sets of stellar models, somewhat different selection criteria in the two samples of stars, and a new metallicity calibration. We use both relations, which are shown in Figure 3*a*, as an indication of the systematic uncertainties in the history of chemical enrichment. The points plotted in this diagram are based on some preliminary results kindly made available by Dr. Ray Carlberg, and differ slightly from the final values.

We make the comparison between models and observations in terms of Z/Z_1, the metallicity normalized to its present value in the interstellar medium in the solar neighborhood. Based on an extrapolation of the relations derived by Twarog (1980) and Carlberg *et al.* (1984) to zero age, we adopt [Fe/H]$_1 = 0.07$, or equivalently $Z_1 = 1.18 \, Z_\odot \approx 0.022$. Since the results of the models are expressed in terms of Z/y, each one implies a particular value of the yield when combined with the adopted value of Z_1. The models also require the present age of the disk, t_1, as an input parameter. As a reasonable compromise between the two age calibrations of the oldest stars in Twarog's sample, we adopt $t_1 = 15$ Gyr. This is consistent with recent estimates of the ages of globular clusters by Janes and Demarque (1983) and Vandenberg (1983).

Another constraint on chemical enrichment in the solar neighborhood is provided by the distribution of metallicities among stars with lifetimes exceeding the age of the disk. As in Paper I, we use the relation derived by Pagel and Patchett (1975) from the ultraviolet excesses of an unbiased sample of 133 G dwarfs. For the present work, we have combined the bins of the original histogram in pairs to obtain the results shown in Figure 3*b*. The scaling of the observational data to Z/Z_1 is based on a metallicity of [Fe/H] $= 0.15$ for the Hyades. For comparison with the observations, the model distribution $dN_s/d \log Z$ is first convolved with a Gaussian in $\log Z$ of dispersion $\delta = 0.15$ to account for the intrinsic and observational scatter in the metallicities at a given age.

For the rest of the disk, we essentially only have information on the present variation of metallicity with galactocentric

radius. The first of the three relations used here is based on the oxygen abundances in H II regions with measured electron temperatures. We obtain a large sample by combining the observations from Shaver *et al.* (1983), Peimbert, Torres-Peimbert, and Rayo (1978), Hawley (1978), and Talent and Dufour (1979). For consistency, all corrections for temperature fluctuations within individual H II regions are taken to be zero. Treating each measurement as independent gives 32 data points, which are then binned in five groups of approximately equal size. The second relation between metallicity and galactocentric radius is that of Harris (1981) for classical Cepheids. Since these stars are all young, their metallicities should be representative of the interstellar medium in the recent past. The third relation, that of Janes (1979), is based on K giants and open clusters in roughly equal proportions. The open clusters are fairly young, whereas the K giants are a mix of all ages, but there is no significant difference in their metallicity gradients. The abundances of heavy elements in each sample of objects are normalized to our estimate of the value in the solar neighborhood. This removes any differences in the zero-points of the metallicity scales and minimizes the effects of any age spread in the samples. As shown in Figure 3d, the three relations for different kinds of objects agree remarkably well, the mean gradient being $d \log Z/dr = -0.06 \pm 0.01$ kpc^{-1}.

d) Variation in the Star Formation Rate

Some constraints can be placed on the history of star formation in the solar neighborhood. From the age distribution in his sample of F dwarfs, Twarog (1980) estimates $1 \lesssim \bar{\psi}/\psi_1 \lesssim 3$ for the ratio of the past averaged to the present rate of star formation, while from the condition that the IMF be smooth near the present main-sequence turnoff, Miller and Scalo (1979) infer $0.4 \lesssim \bar{\psi}/\psi_1 \lesssim 3$, for $t_1 = 15$ Gyr. Both of these estimates assume a constant IMF.

The variation of the present rate of star formation with galactocentric radius can be inferred from a variety of radio observations, again on the assumption of a constant IMF. As in Paper I, we use the distribution of pulsars from Lyne, Manchester, and Taylor (1984), supernova remnants from Guibert, Lequeux, and Viallefond (1978) and Lyman-continuum photons from Mezger (1978) as tracers of recent star formation. Since the absolute value of the star formation rate cannot be derived from these observations without assuming an IMF, as well as mass ranges for producing pulsars, supernovae, etc., all of which are poorly known, we express each radial distribution relative to its value in the solar neighborhood in the form $\psi(r)/\psi_1$. The results derived in this way and shown in Figure 3c are reasonably consistent with each other and have a roughly exponential dependence on radius, with a scale length of 3 ± 1 kpc, over the range $4 \lesssim r \lesssim 12$ kpc.

There have been many attempts to test the validity of the relation $\psi \propto \mu_g{}^m$ by comparing the distributions of atomic hydrogen and tracers of star formation in other galaxies (Hamajima and Tosa 1975, and references therein). However, the inferred values of m are likely to be modified significantly when the contributions from molecular hydrogen are included. For our own Galaxy, a plot of the star formation rate against the surface density of gas, using the data assembled in this paper, suggests $m \approx 2$ over the range 3 kpc $\lesssim r \lesssim 12$ kpc, but the uncertainty is large and $m = 1$ is not ruled out. This appears to be consistent with the limits $1.3 \lesssim n \lesssim 2$ on the Schmidt exponent derived by Guibert *et al.* from earlier observations since the scale height of the gas layer increases grad-

ually with distance from the galactic center. The constraints on the past variation of the star formation rate in the solar neighborhood mentioned above, and similar constraints derived for other galaxies, have been used to argue that m and n cannot even be as large as 1 (Miller and Scalo 1979; Kennicutt 1983). However, such arguments are all based on the assumption of closed system evolution and do not apply to models with infall or radial flows.

e) Constraints on the Infall and Radial Flow Rates

The high-velocity clouds of atomic hydrogen have sometimes been taken as evidence for infall, although this explanation is controversial. Oort (1970) supposed that the clouds were ejected from the disk and were then pushed back by diffuse gas streaming into the Galaxy from outside. In this way he estimated an infall rate of $f_1 \approx 2$ $M_\odot$ pc^{-2} Gyr^{-1} for the solar neighborhood, which corresponds roughly to $\dot{M}_D \approx 2$ $M_\odot$ yr^{-1} for the Galaxy as a whole. The diffuse gas would almost certainly be highly ionized and would emit X-rays in a cooling flow as it approached the disk. From a set of detailed hydrodynamical calculations and observations of the soft X-ray background, Cox and Smith (1976) derived a rough upper limit of $\dot{M}_D \lesssim 1$ $M_\odot$ yr^{-1} on the present infall rate.

An alternative interpretation of the high-velocity clouds is in terms of a galactic fountain (Bregman 1980 and references therein), in which hot gas rises up several kpc from the disk and then condenses into clouds that fall back toward the plane. If the clouds return to the original position of the gas in the disk, the standard equations of chemical evolution require no modification, but if they reenter at larger galactocentric radii, their mixing in the gas layer would induce a radial inflow. Unfortunately this process is not yet understood well enough to be included in models of chemical evolution, even though it could affect the results. Moreover, the fountain model may have difficulty in accounting for the preponderance of negative radial velocities in the direction of the galactic center recently observed by Mirabel and Morras (1984). They suggest that the clouds with the highest velocities represent the accretion of neutral gas from outside the Galaxy, at a rate of $\dot{M}_D \approx 0.2$ $M_\odot$ yr^{-1} if the typical distances are 20 kpc.

The problem of estimating the radial velocity of the gas in the disk of our Galaxy splits into two parts: the determination of the local standard of rest (LSR) for circular orbits, and the determination of the radial motion of the gas with respect to the LSR. Most radio observations are expressed relative to a "standard" LSR, which coincides approximately with the mean motion of the nearby bright stars (see, e.g., Kerr 1969). However, this frame of reference may not coincide with the true LSR as a result of the influence of a density wave on the motions of the stars. From an analysis of such effects, Wielen (1979) argues that the standard LSR has an outward motion of about 6 km s^{-1} relative to the local circular velocity. Moreover, Kerr (1962) and Henderson, Jackson, and Kerr (1982) point out that the galactic rotation curve and H I distribution derived from 21 cm observations would be more symmetric between north and south if the standard LSR had a similar outward motion of 7–10 km s^{-1}.

The local H I appears to be at rest relative to the standard LSR to within about 1 km s^{-1} (Kerr 1969; Crovisier 1978). According to Radhakrishnan and Sarma (1980), the mean radial velocity of the H I absorption features along the line-of-sight to the galactic center also closely coincides with that of the LSR. Within 3–4 kpc of the galactic center, however, there

are large noncircular motions in the gas, which may result from explosions or from the gravitational field of a bar (as reviewed by Oort 1977). In the latter case, the net radial flow, averaged around an orbit, might be either inward or outward. In the anticenter direction, the H I emission features at low latitudes have a mean inward motion relative to the LSR of about 3.5 km s^{-1} (Velden 1970). For the molecular clouds within a few kpc of the Sun, Stark (1984) finds a mean inward motion of roughly 4 km s^{-1}. Thus although the situation is somewhat confused by the uncertainty in the LSR, the available observations indicate that there may be gas flows in the disk with radial velocities of up to $|v_r| \lesssim 5$ km s^{-1}, and that these flows are more likely to be inward than outward over most of the disk.

IV. RESULTS OF THE MODELS

a) Method of Presentation

We present results for a series of models, which are designated A to X, in Table 1 and in Figures 3–8. Table 1 gives the values of the adjustable input parameters for each model: the star formation exponent m and coefficient C, the form of the radial velocity field and its value in the solar neighborhood v_0, the infall time scale τ and scale length α_f^{-1}, and the star formation cutoff radius r_*. Also listed in the table are the values of some output parameters from the models: the present solar neighborhood values Z_1/y, μ_{g1}, μ_{s1}, and $\bar{\psi}/\psi_1$; the infall and net star formation rates for the Galaxy as a whole, $\dot{M}_D$ and $(1 - R)\Psi$; the gas depletion time scale $\tau_g = M_g/[(1 - R)\Psi - \dot{M}_D]$; and finally the mass of the disk within 1 kpc of the center, $M_D(r < 1$ kpc). In the figures, we show the relations $\log Z(t)$ and $dN_s(Z)/d \log Z$ for the solar neighborhood, and the relations $\log \psi(r)$, $\log Z(r)$, $\log \mu_s(r)$, and $\log \mu_g(r)$ at the present time for $0 \leq r \leq 20$ kpc. This format allows a

direct comparison between the theoretical models and the observational constraints.

The results are governed by infall, radial flows, the presence or absence of an edge in the stellar disk, and the exponent in the star formation rate. We have chosen some of the models to illustrate these effects separately and some of them to illustrate various interactions between the effects. Only models with radial inflows are presented here, since a few computations of models with outflows indicated that they cannot explain abundance gradients in the form observed. We discuss the results for $m = 1$ and $m = 2$ separately, because the character of the results is sensitive to the dependence of the star formation rate on gas density. If we rewrite equation (3) in terms of the time derivative comoving with the gas flow, we obtain

$$DZ/Dt \equiv [(\partial/\partial t) + (v_r \, \partial/\partial r)]Z = [y(1 - R)\psi/\mu_g] - (Zf/\mu_g) \, .$$

(14)

This shows that the evolution of the metallicity reflects a competition between the efficiency of star formation, ψ/μ_g, and the dilution by infall, f/μ_g. The efficiency of star formation may vary with radius continuously because of its dependence on gas density, or discontinuously because there is an edge to the stellar disk. With a constant infall time scale, the dilution may vary with radius either because of redistribution of gas by radial flows or because of differential depletion of gas by star formation. In the former case, dilution will produce or enhance a metallicity gradient, whereas in the latter case, it will tend to reduce the gradient caused by variations in the efficiency of star formation. In more general models than those presented here, the infall time scale might depend on radius, and in this case also, a metallicity gradient would develop because of the variation of the dilution with radius.

TABLE 1
INPUT AND OUTPUT PARAMETERS FOR THE MODELS

Model	m	C	Velocity Field	v_0	τ	α_f^{-1}	r_*	Z_1/y	μ_{g1}	μ_{s1}	$\bar{\psi}/\psi_1$	$\dot{M}_D$	$(1 - R)\Psi$	τ_g	$M_D(r < 1$ kpc$)$
A	1	0.1	...	0	0	4	∞	1.50	16	55	2.3	0.0	1.3	10	0.2
B	1	0.2	...	0	6	4	∞	1.38	13	59	1.6	0.9	2.1	8.7	0.2
C	1	0.1	a	-1	0	4	∞	1.50	1.1	27	16	0.0	1.3	10	3.3
D	1	0.2	a	-1	6	4	∞	0.83	5.2	37	2.4	0.9	2.1	8.7	2.0
E	1	0.1	a	-1	0	4	18	0.97	1.9	28	9.9	0.0	1.4	10	3.3
F	1	0.2	a	-1	6	4	18	0.84	5.5	38	2.3	0.9	2.2	9.0	2.0
G	1	0.2	a	-0.5	6	4	18	1.09	7.9	46	2.0	0.9	2.1	9.7	1.1
H	1	0.2	a	-2	6	4	18	0.48	3.2	27	2.8	0.9	2.2	8.7	3.2
I	1	0.2	b	-1	6	6	∞	0.97	8.3	52	2.1	0.9	2.1	8.7	0.3
J	1	0.2	b	-1	6	6	18	0.91	10	55	1.8	0.9	2.3	8.8	0.3
K	1	0.2	c	-1	6	4	∞	0.84	4.7	34	2.4	0.9	2.1	8.7	2.7
L	1	0.2	c	-1	6	4	18	0.85	4.7	34	2.4	0.9	2.1	9.9	2.7
M	2	0.005	...	0	0	4	∞	1.85	11	60	6.3	0.0	0.4	26	0.2
N	2	0.01	...	0	3	4	∞	1.66	9.9	61	4.2	0.14	0.8	17	0.2
O	2	0.005	a	-0.5	0	4	∞	0.77	9.7	53	7.5	0.0	0.5	14	0.6
P	2	0.01	a	-0.5	3	4	∞	1.02	9.5	56	4.1	0.14	0.8	12	0.5
Q	2	0.01	a	-1	3	4	∞	0.44	6.6	46	6.9	0.14	0.8	7.9	0.9
R	2	0.01	a	-2	3	4	∞	0.05	1.9	27	51	0.14	0.6	4.1	1.9
S	2	0.01	a	-1	3	6	∞	0.80	9.6	52	3.8	0.14	1.1	11	0.7
T	2	0.01	a	-0.5	3	4	18	1.02	9.5	56	4.1	0.14	0.8	12	0.5
U	2	0.005	b	-0.5	0	6	∞	1.03	18	72	3.1	0.0	0.9	12	0.1
V	2	0.01	b	-0.5	3	6	∞	1.37	14	71	2.5	0.14	1.1	11	0.1
W	2	0.01	c	-0.5	3	4	∞	1.01	7.9	48	5.1	0.14	0.8	13	0.9
X	2	0.01	d	-0.5	3	4	18	1.02	9.5	56	4.1	0.14	0.8	12	1.9

NOTES.—(1) All models were computed with $t_1 = 15$ Gyr and $M_D(t_1) = 6 \times 10^{10} \, M_\odot$. (2) Model X has $v_1 = -10$ km s^{-1}. (3) Units: C in $(M_\odot \, \mathrm{pc}^{-2})^{1-m}$ Gyr^{-1}, v_0 in km s^{-1}, τ and τ_g in Gyr, α_f^{-1} and r_* in kpc, μ_{g1} and μ_{s1} in $M_\odot$ pc^{-2}, $\dot{M}_D$ and $(1 - R)\Psi$ in $M_\odot$ yr^{-1}, $M_D(r < 1$ kpc$)$ in $10^{10} \, M_\odot$.
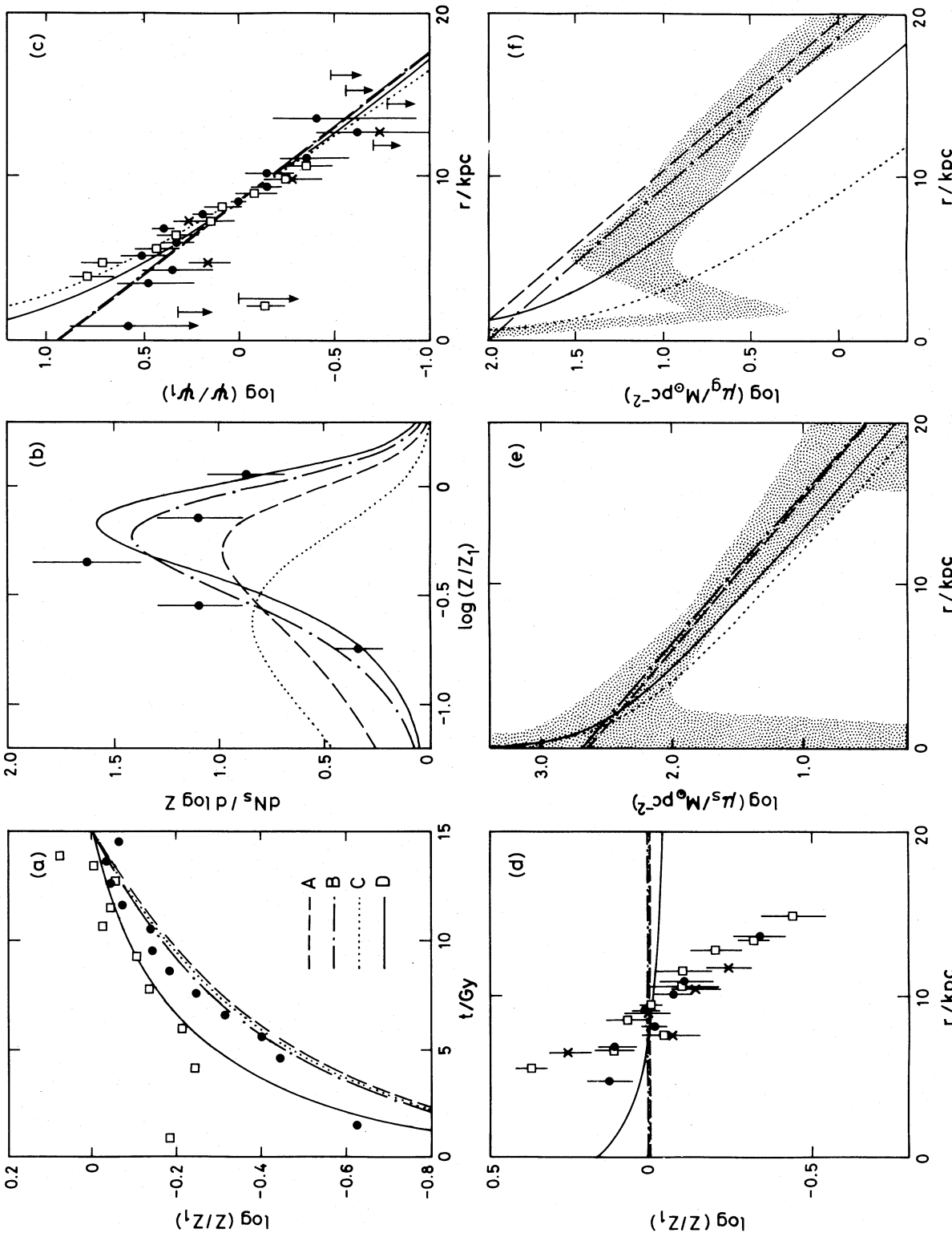
FIG. 3.—Comparison of predictions for models A, B, C, D with observations. (a) Metallicity as function of age for stars in solar neighborhood; data from Twarog (1980) (*filled circles*) and Carlberg *et al.* (1984) (*open squares*). (b) Normalized distribution of metallicities for G dwarfs in solar neighborhood. Data from Pagel and Patchett (1975); error bars represent $N^{1/2}$ uncertainties. (c) Present radial variation of star formation rate; data from Lyne, Manchester, and Taylor (1984), based on pulsars (*filled circles*), Guibert, Lequeux, and Viallefond (1978), based in supernova remnants (*crosses*), and Mezger (1978), based on Lyman continuum (Lyc) emission (*open squares*); errors bars represent $N^{1/2}$ uncertainties for pulsars and SNRs and are our own estimates for Lyc emission. (d) Present radial variation of metallicity; data from Shaver *et al.* (1983) and others, based on H II regions (*crosses*), Harris (1981), based on Cepheids (*open squares*), and Janes (1979), based on K giants and open clusters (*filled circles*). (e) Present radial variation in the surface density of stars; shaded region represents estimated range derived as explained in text and is only schematic near the center. (f) Present radial variation in the surface density of gas; shaded region represents estimated range derived from observations in Fig. 2.
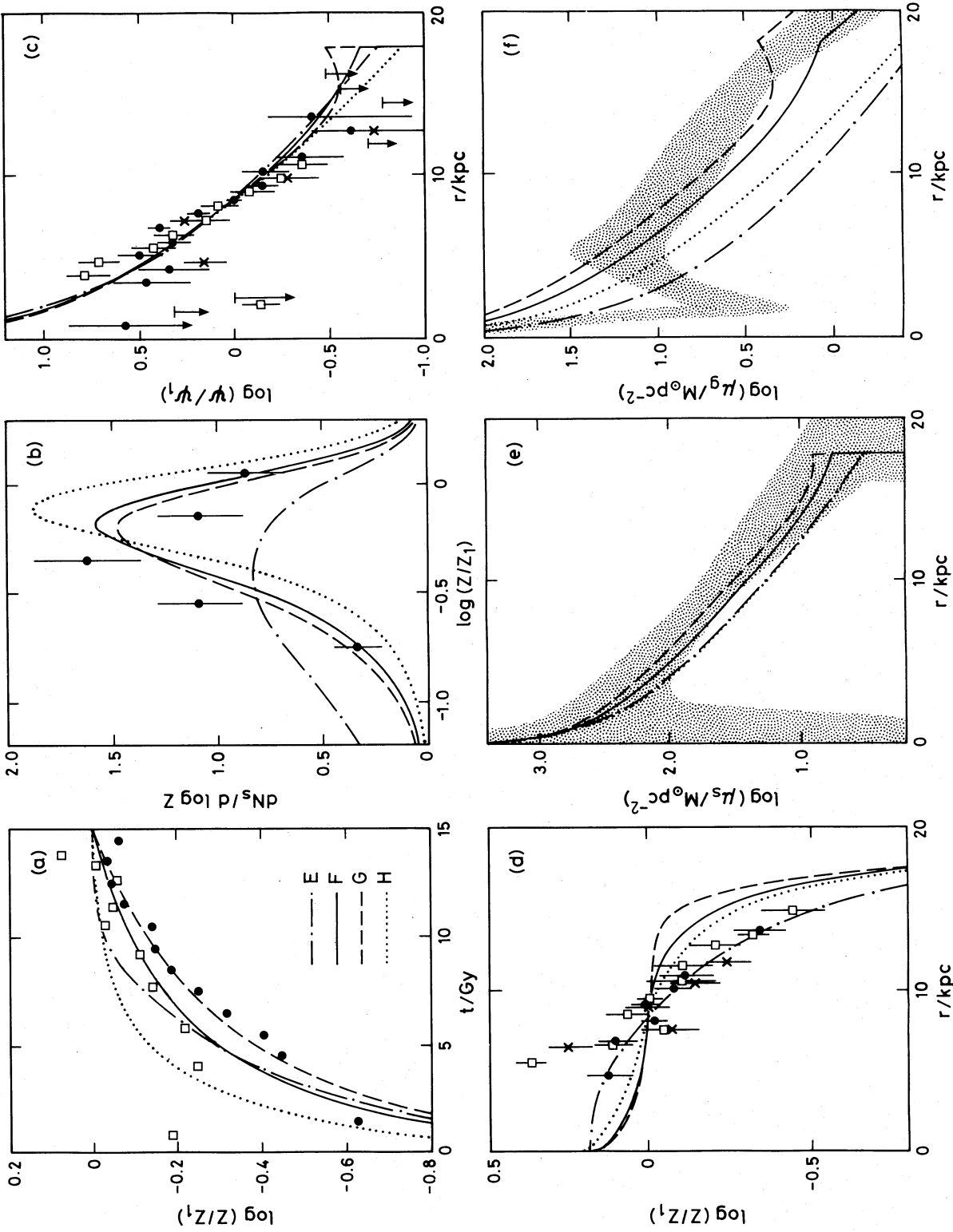
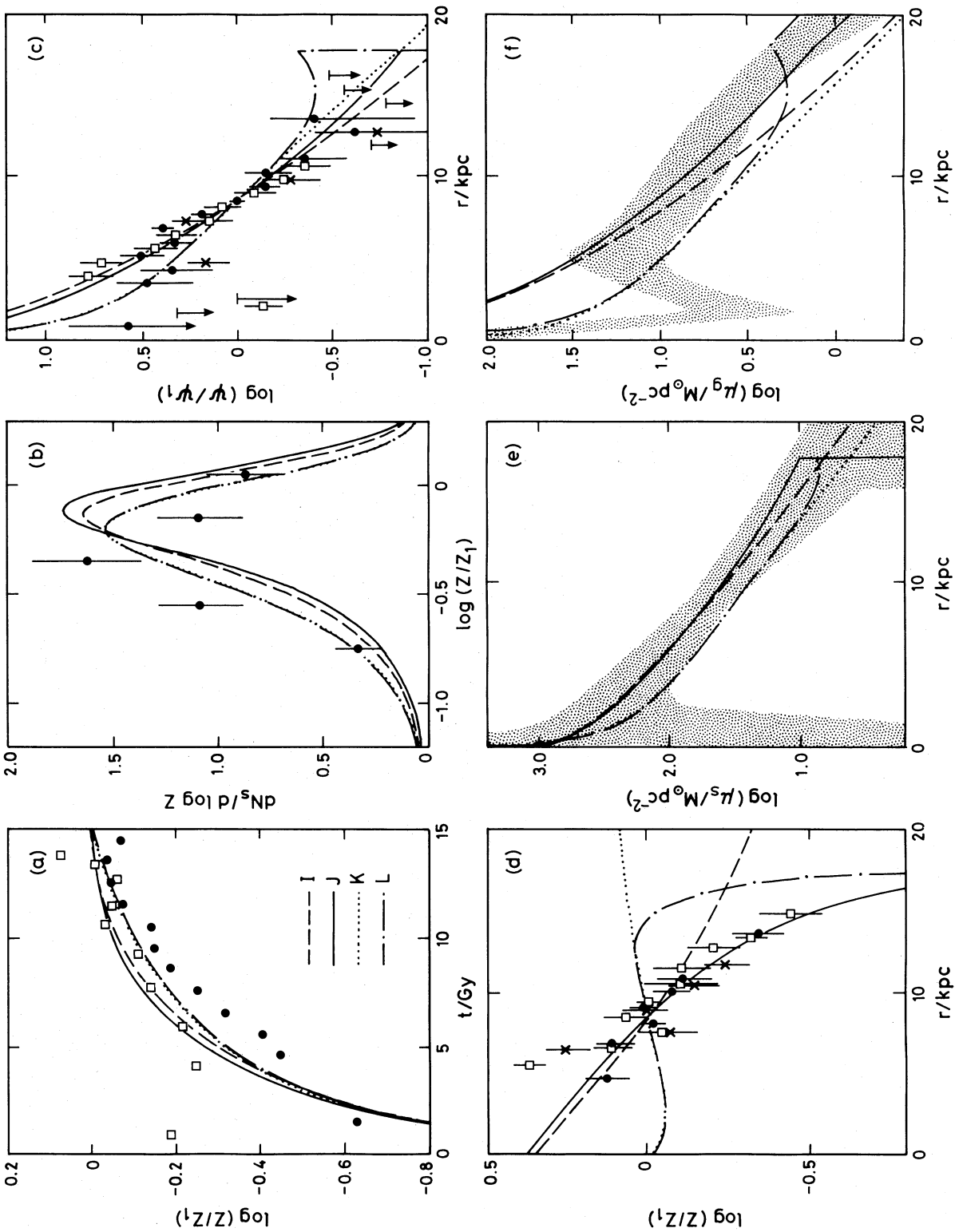FIG. 4.—Same as Fig. 3, but for models E, F, G, H

162

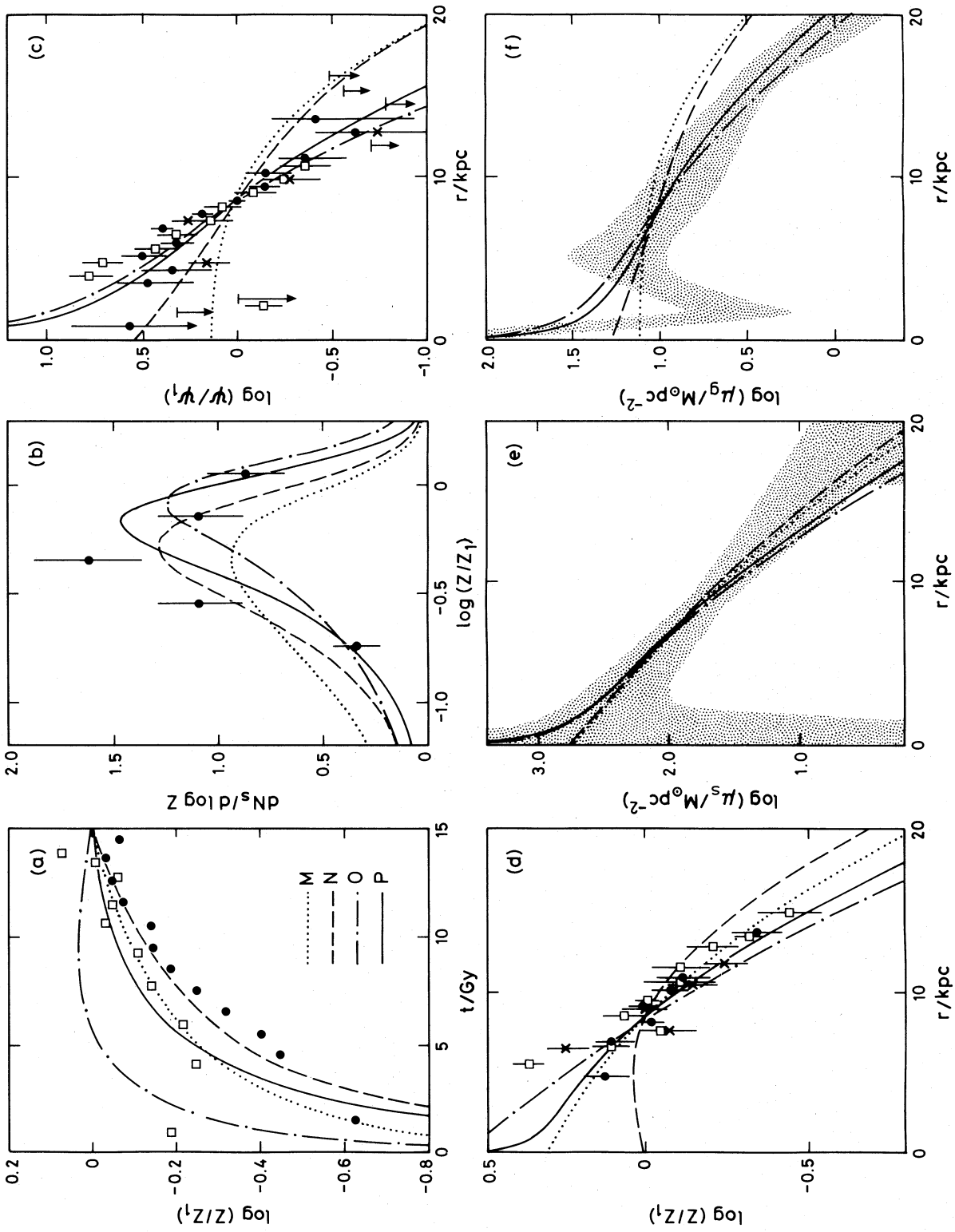FIG. 5.—Same as Fig. 3, but for models I, J, K, L

163

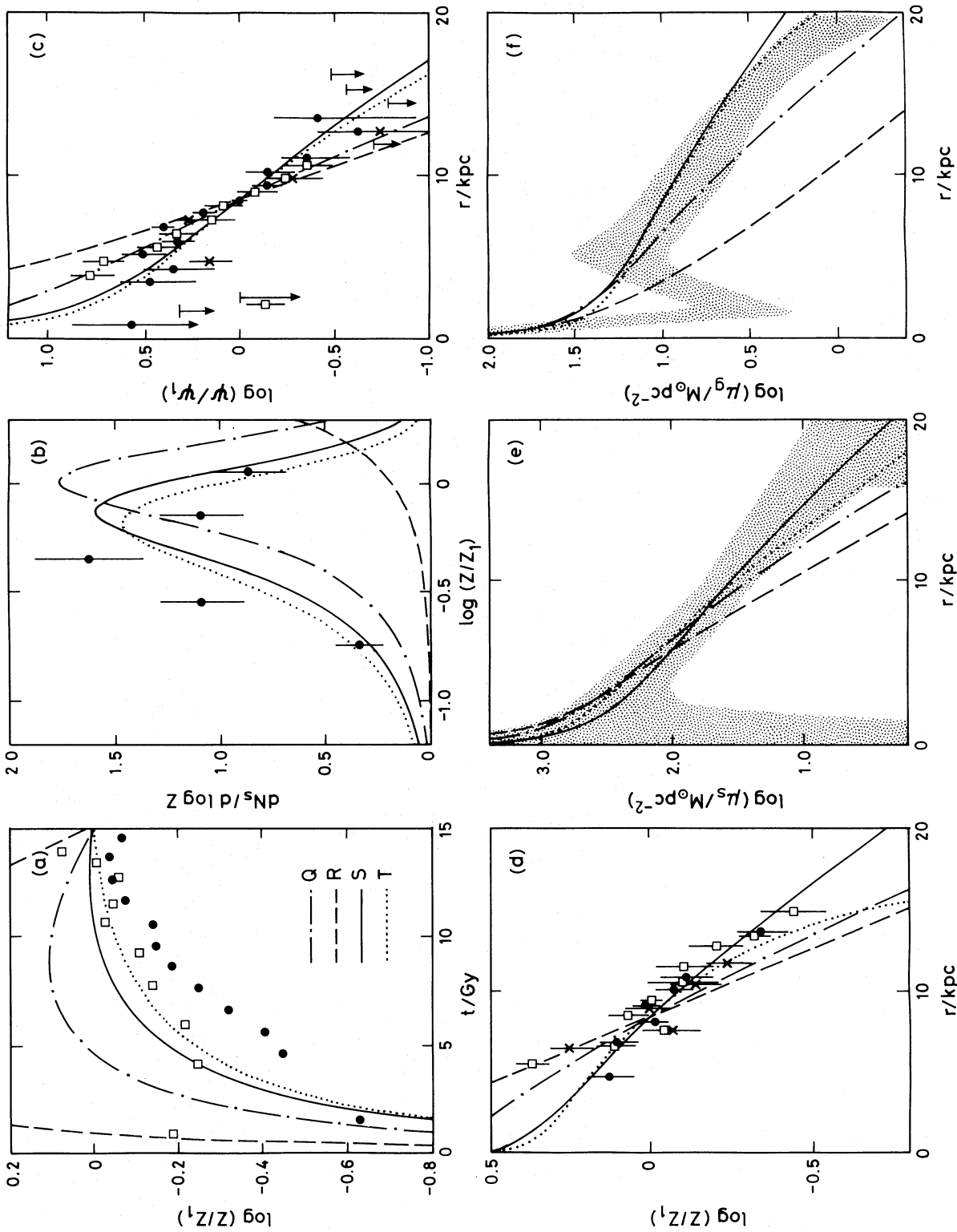FIG. 6.—Sames as Fig. 3, but for models M, N, O, P

164

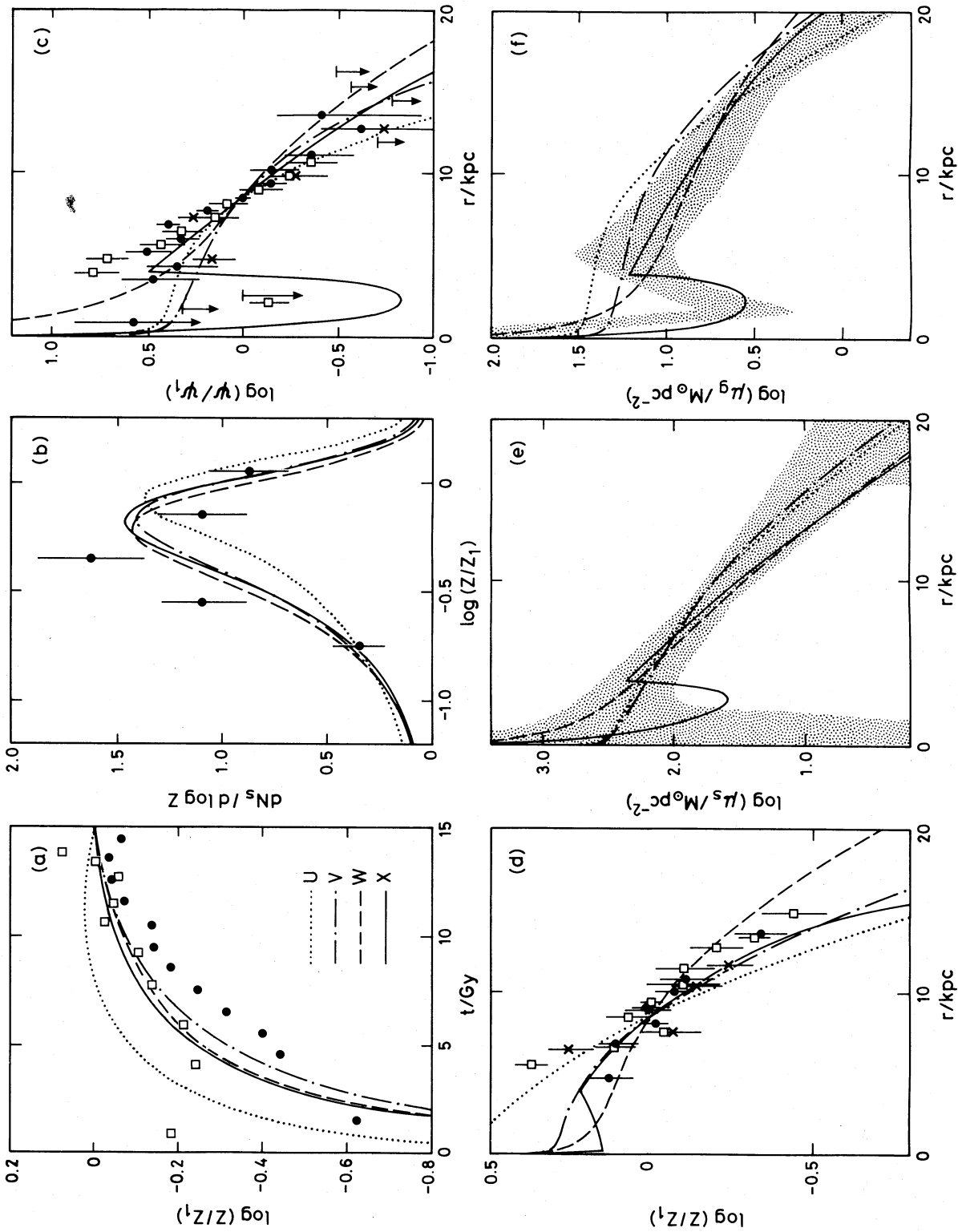Fig. 7.—Same as Fig. 3, but for models Q, R, S, T

Fig. 8.—Same as Fig. 3, but for models U, V, W, X

For models with $m = 1$, the efficiency of star formation ψ/μ_g is independent of gas density, so that, in the absence of inflows and edges, f/μ_g is also independent of radius and there are no gradients in the gas fraction or chemical abundance. Inflow combined with infall produces a metallicity gradient through the dilution term f/μ_g; the value of Z is increased at radii where the inflow raises the gas density, and vice versa. Inflow also produces a metallicity gradient when combined with a star formation edge: the discontinuity in Z is then spread out by the inflow into a smooth gradient over a finite part of the disk.

For models with $m = 2$, the efficiency of star formation varies with gas density as $\psi/\mu_g \propto \mu_g$. Therefore, in the absence of infall and radial flows, the gas fraction decreases and the metallicity increases with decreasing galactocentric radius. Infall flattens the metallicity gradient because dilution is more effective where the gas has been more depleted by star formation. Inflow tends to raise the gas density at small radii, thus counteracting the dilution by infall and steepening the metallicity gradient. In comparison with these effects, star formation edges play only a minor role in models with $m = 2$.

We have calculated the abundance of secondary elements S in the models on the assumption that they are produced in proportion to the abundance of primary elements (e.g., Tinsley 1980). In this case, the evolution equation for S is the same as equation (3) for Z, except that $y(1 - R)\psi$ is replaced by $y_s(Z/y) \times (1 - R)\psi$. We find that the limits $\frac{1}{2} \le (S/y_s)/(Z/y)^2 \le 1$ hold at all times, at all radii and in all models. The lower bound of this range applies to closed models, with $f = 0$, while the upper bound applies to extreme infall models, with $f = (1 - R)\psi$ (cf. Tinsley 1980). For most of our models, the relation $S \propto Z^2$ predicted by the simple model of chemical evolution is obeyed even more closely than required by the above inequalities, departures from proportionality being associated with variations in the importance of infall relative to star formation. A more complete account of these results is given by Lacey (1984). There have been many empirical tests of the relation $S \propto Z^2$ (see, e.g., Tinsley 1980; Pagel and Edmunds 1981), so we do not discuss the observations here, except to note that many of them do not follow the theoretical prediction.

b) Models with $m = 1$

The first two models with $m = 1$ have no inflows, and differ mainly in the time scale of infall: $\tau = 0$ for model A and $\tau = 6$ Gyr for model B. They can account for the age-metallicity relation in the solar neighborhood and the present radial variations in the surface densities of stars and gas and in the star formation rate. With infall, the metallicity distribution in the solar neighborhood is acceptable, but neither model has an abundance gradient. Models C and D are the same as models A and B, respectively, except that they include inflow at a constant velocity of $v_r = -1$ km s^{-1}. This reduces μ_g and μ_s at all radii except near the center, while leaving the relative variation with radius little changed. The metallicity evolution is also little changed. In the absence of infall, the solution of equation (14) is $Z/y = Ct$, and there is no metallicity gradient, with or without inflow. The metallicity distribution is, however, shifted to lower values of Z/Z_1 because of the large reduction in μ_g, and thus ψ, at recent times. Thus inflow makes the G dwarf problem worse when there is no infall, although this can be counteracted to some extent by increasing the scale length $\alpha_f{}^{-1}$. When infall is present, the curvature in the age-metallicity relation increases, and Z eventually tends to a steady state value. A weak abundance gradient develops because the dilution term is smaller near the center.

The effects of an edge in the stellar disk are illustrated by models E and F, which are modifications of models C and D, respectively, to include star formation cutoffs at $r_* = 18$ kpc. For models without infall such as E, it is simple to show, again using equation (14), that over a distance $|v_r|t$ inside the edge, Z/y is constant in time and linear in radius with a gradient $-C/|v_r|$; nearer the center, Z/y is constant with radius but increases with time as $Z/y = Ct$. Thus the metallicity gradient propagates inwards from the edge until, after a crossing time $r_*/|v_r|$, a steady state gradient covers the entire stellar disk. When infall is combined with inflow, as in model F, the final metallicity gradient extends inward only by a few scale lengths, but, in the cases of interest, this is enough to reach most of the way to the center after about a crossing time.

Models G and H are the same as model F apart from the value of the inflow velocity, which is $v_r = -0.5$ km s^{-1} in the first case and $v_r = -2$ km s^{-1} in the second case. The progression G, F, H illustrates the following general features: The metallicity gradient $d \log Z/dr$ is not sensitive to the inflow velocity for $|v_0| \gtrsim 1 - 2$ km s^{-1}, whatever the form of $v_r(r)$ and whether or not there is infall or an edge. However, for models with infall and/or an edge, the overall level of enrichment, as measured by Z_1/y, falls with increasing inflow velocity, roughly as $1/|v_0|$ for large $|v_0|$, as does the time for the age-metallicity relation to flatten off. With infall, the gradients in μ_s, μ_g, and ψ are not sensitive to increases in the inflow velocity for $|v_0| \gtrsim 0.5$ km s^{-1}, except near the edge and near the center, but the overall levels of these quantities are reduced, μ_g and ψ quite rapidly, as $|v_0|$ rises. The metallicity distribution in the solar neighborhood is not sensitive to the inflow velocity for $|v_0| \gtrsim 1-2$ km s^{-1} when there is infall, but for larger inflow velocities the distribution shifts to larger values of Z/Z_1 because the age-metallicity relation flattens off at early times.

We next consider different velocity fields for the inflow. Since the evolution of Z for models without infall is similar whatever the form of $v_r(r)$, only the results with infall are presented here. Model I, without an edge, and model J, with an edge, demonstrate the effects of a radially increasing inflow velocity, with $v_0 = -1$ km s^{-1}. They are similar to models D and F respectively, except that $\alpha_f{}^{-1}$ is increased from 4 to 6 kpc to obtain a better fit to the radial variation in μ_g, μ_s, and ψ. Model I has a larger metallicity gradient than model D because of the greater radial variation of the dilution term f/μ_g, which results from the steepening of the radial gradient in the gas density for this velocity field. In model J, the metallicity rises less steeply near the edge and more steeply near the center, as compared with model F. Models K and L show the effects of a radially decreasing inflow velocity with $v_0 = -1$ km s^{-1}, but they are otherwise the same as models D and F, respectively. A small positive metallicity gradient develops through dilution by infall because the inflow flattens the density profile of the gas. Model L, with an edge, has a steeper variation of Z near the edge than model F, but, like model K, also has a positive gradient near the center.

c) Models with $m = 2$

The results from model M, without infall, and model N, with infall on a time scale $\tau = 3$ Gyr, are typical of models with $m = 2$ and no radial flows. In the absence of infall, the metallicity gradient is acceptable, but the fraction of metal-poor stars is too large, whereas in the presence of infall, the metal-

licity distribution is acceptable, but the metallicity gradient is too flat. Another problem with these models is that the radial distributions of gas and star formation are too flat, particularly when there is no infall, although they do reproduce the observed age-metallicity relation. Models O and P are the same as models M and N respectively, except that they include inflow at a constant velocity of $v_r = -0.5$ km s^{-1}, which causes a steepening in the radial gradients of the gas density, star formation rate, and metallicity. The curvature in the age-metallicity relation is increased because the gas presently in the solar neighborhood was originally at larger radii and therefore had a lower efficiency of star formation, and correspondingly, the peak in the metallicity distribution is shifted to higher values of Z/Z_1. These effects are largest in models without infall such as model O, for which inflow can solve the G dwarf problem, but only at the expense of giving the age-metallicity relation too much curvature compared to the observations.

Models Q and R illustrate the effects of increasing the inflow velocity, to $v_r = -1$ km s^{-1} and $v_r = -2$ km s^{-1}, respectively; otherwise they are the same as model P. This increases the curvature in the age-metallicity relation, which peaks at some time before the present, and shifts the metallicity distribution to higher values of Z. The radial gradients in μ_s, μ_g, ψ, and Z are steepened somewhat, but they are not very sensitive to $|v_0|$. The overall levels of μ_g, ψ, and Z/y, however, decrease quite rapidly with increasing $|v_0|$, whatever the form of $v_r(r)$. Model S, which is similar to model Q, shows that many of the effects of increasing the inflow velocity can be partially offset by increasing the scale length α_f^{-1}, in this case from 4 kpc to 6 kpc. Model T is the same as model P except that it has a star formation cutoff and therefore a steeper metallicity gradient near the edge.

We now consider the results for different velocity fields. Model U, without infall, and model V, with infall, are the same as models O and P, respectively, apart from the rising inflow velocity field with $v_0 = -0.5$ km s^{-1}, and an infall scale length of 6 kpc. The radially increasing velocity field considerably steepens the gradients in μ_g, ψ, and Z, except near the center, but this is counteracted to some extent by the larger value of α_f^{-1}. Model W is the same as model P, apart from an inflow velocity that decreases outward. Larger inflow velocities lead to further steepening of the gradients in models with the radially rising velocity field, but the gradients are not sensitive to $|v_0|$ when the velocity decreases radially. Finally, we have model X, which is the same as model T except that the inflow velocity rises sharply close to the center. This illustrates how an inner hole in the radial distributions of gas density and star formation can be created by radial inflow. There is a corresponding hole in the stellar disk and also a dip in the metallicity because the dilution by infall is more effective where the gas is depleted.

d) General Results and Implications

For models with $m = 1$, metallicity gradients of the correct sign only develop when inflow is combined with infall or a star formation edge. However, even the most steeply rising velocity field considered here, with $v_r \propto r$, fails to produce a metallicity gradient as large as that observed. It is possible that an even more steeply rising velocity field might account for the observed gradient, but we did not calculate any such models. Inflow combined with a star formation edge can produce a gradient in agreement with observations, whether or not there is infall. However, infall is needed in these models to reproduce

the metallicity distribution in the solar neighborhood together with the radial variation in the gas density. Thus, the best fitting models with $m = 1$, such as model J, have infall, a star formation edge, and inflow with $v_r \propto r$. To match the observations, $|v_0|$ must be close to r_*/t_1, because if it is smaller, the metallicity gradient does not reach to the center, whereas if it is larger, the age-metallicity relation flattens off too early.

For models with $m = 2$, abundance gradients develop even in the absence of inflow, infall, or edges because of the variation of the efficiency of star formation with gas density, which tends to dominate even when the other effects are present. Inflow is needed, however, to steepen the gradients in the gas density and star formation rate, which are otherwise too shallow compared to observations. If there is inflow, then infall is needed to match the age-metallicity relation in the solar neighborhood, although the metallicity distribution can be explained without it. The metallicity gradient is flattened by infall when there are no radial flows but becomes insensitive to infall when inflows are included. The presence of a star formation edge also has little effect on the metallicity gradient. Thus, the best fitting models with $m = 2$, such as models P and X, have infall and inflow with $v_r = $ constant.

The observational uncertainties in the gas density and the star formation rate are such that acceptable fits to all of the data can be found for both $m = 1$ and $m = 2$. Of the models presented here, which were chosen to illustrate effects rather than to optimize fits, the best fitting $m = 1$ model is J, with $\tau = 6$ Gyr, $r_* = 18$ kpc, $v_r \propto r$, and $v_0 = -1$ km s^{-1}, while the best fitting $m = 2$ model is X, with $\tau = 3$ Gyr, $r_* = 18$ kpc, and $v_r = -0.5$ km s^{-1} except for strong inflow at the center. Both of these models satisfy the subsidiary constraints on $\bar{\psi}/\psi_1$ and $\dot{M}_D$ and have reasonable gas depletion time scales $\tau_g \approx 10$ Gyr and star formation rates $(1 - R)\Psi \approx (1-2)$ $M_\odot$ yr^{-1}. They also imply values of the yield $y \approx 0.02$ that agree with the predictions of stellar nucleosynthesis calculations (Arnett 1978; Maeder 1981).

The inclusion of inflows somewhat reduces the infall time scale required, compared to models with no radial flows. This is mainly because, with inflows, consistency with the observational constraints on the radial variation in the gas density and the radial and temporal variations in the star formation rate can be obtained with larger values of m. In this case, the age-metallicity relation and metallicity distribution in the solar neighborhood can be fit with smaller values of τ. Thus acceptable fits can be found for $\dot{M}_D \gtrsim 0.1$ $M_\odot$ yr^{-1}, compared to $\dot{M}_D \gtrsim 1$ $M_\odot$ yr^{-1} for the models without inflows in Paper I. The infall time scale and the present infall rate might be further reduced by the delayed ejection of matter from low-mass stars, which is neglected in the approximation of instantaneous recycling. It would be useful to check these results with calculations that include finite stellar lifetimes.

The gradients in log μ_s, log μ_g, log ψ, and log Z are generally not sensitive to the magnitude of the inflow velocity for $|v_0| \gtrsim 1$ km s^{-1}, but the overall levels of the latter three quantities decline quite rapidly with increasing $|v_0|$. In particular, the gas density provides a strong constraint on $|v_0|$, as does the form of the age-metallicity relation in models with $m = 2$. After allowing for variations in the scale length α_f^{-1} of the infall, in which case the gradients in stellar density, gas density, and star formation rate also enter as important constraints, we estimate $|v_0| \lesssim 2$ km s^{-1} as a rough upper limit, if the inflow velocity has been constant over the life of the Galaxy. In reality, v_r may have varied with time, and the previous limit would then apply

to some average value that is weighted to the recent past. Our predicted dependence of the radial gradient and overall level of enrichment on the inflow velocity also may be consistent with observations of other spiral galaxies. If strongly barred systems are excluded, the metallicity gradients, when scaled by the photometric radii, are similar in different galaxies, while the overall level of the metallicity varies somewhat between galaxies (Pagel and Edmunds 1981; Webster and Smith 1983).

V. CONCLUSIONS

1. Radial gas flows at velocities as small as $|v_r| \sim 1$ km s^{-1} have important effects on the chemical evolution of the galactic disk. Velocities of this magnitude are expected on theoretical grounds and are consistent with the available observations. However, the present constraints are weak and further studies of radial flows, both theoretical and observational, would be desirable. In the absence of spatial or temporal variations in the IMF, radial gas flows are probably required to explain the metallicity gradient in the galactic disk.

2. Metallicity gradients can arise from radial variations in either the efficiency of star formation or in the efficiency of dilution by infall. For models with $m = 1$, the observed gradient is reproduced by a combination of inflow and a star formation edge; a good fit to all of the data is obtained with $v_r \propto r$, $v_0 = -1$ km s^{-1}, $r_* = 18$ kpc, and $\tau = 6$ Gyr. For models with $m = 2$, abundance gradients result mainly from the variation in the efficiency of star formation with gas density; a good fit to all of the data is obtained with $v_r =$ constant $= -0.5$ km s^{-1} and $\tau = 3$ Gyr.

3. Infall is required to fit the observations even when radial inflows are included in the models. For $m = 1$, infall at a total rate $\dot{M}_D \approx 1$ $M_\odot$ yr^{-1} is mainly needed to reproduce the metallicity distribution in the solar neighborhood, whereas for $m = 2$, infall at the lower rate $\dot{M}_D \approx 0.1$ $M_\odot$ yr^{-1} is required to fit the age-metallicity relation. These estimates, and the corresponding infall time scale may be reduced somewhat when the approximation of instantaneous recycling is relaxed.

4. The gradients in the metallicity, gas density, and star formation rate are generally not sensitive to increases in the inflow velocity for $|v_r| \gtrsim 1$ km s^{-1}, but the overall levels of these quantities decrease fairly rapidly with increasing $|v_r|$. This may account for some of the observed variations in the chemical abundances between different spiral galaxies. From the models we estimate an upper limit on the inflow velocity in the disk of our Galaxy, assuming that it is roughly constant in time, to be $|v_0| \lesssim 2$ km s^{-1}.

5. If the infall rate increases smoothly in to the center of the Galaxy, the depression in the gas density and star formation rate at $1 \lesssim r \lesssim 4$ kpc may be explained by enhanced inflow near the center, at a velocity of $v_r \sim -10$ km s^{-1}. This depresses the metallicity in the same region and builds up a concentration of mass at the galactic center.

REFERENCES

Arnett, W. D. 1978, *Ap. J.*, **219**, 1008.
Bahcall, J. N. 1984, *Ap. J.*, **276**, 169.
Bahcall, J. N., Schmidt, M., and Soneira, R. M. 1983, *Ap. J.*, **265**, 730.
Bahcall, J. N., and Soneira, R. M. 1980, *Ap. J. Suppl.*, **44**, 73.
Baker, P. L., and Burton, W. B. 1975, *Ap. J.*, **198**, 281.
Blitz, L., Fich, M., and Kulkarni, S. 1983, *Science*, **220**, 1233.
Bregman, J. N. 1980, *Ap. J.*, **236**, 577.
Burton, W. B., and Gordon, M. A. 1978, *Astr. Ap.*, **63**, 7.
Caldwell, J. A. R., and Ostriker, J. P. 1981, *Ap. J.*, **251**, 61.
Carlberg, R. G., Dawson, P. C., Hsu, T., and Vandenberg, D. A. 1984, *Ap. J.*, submitted.
Chandrasekhar, S. 1960, *Principles of Stellar Dynamics* (2d ed.; New York: Dover).
Chromey, F. R. 1978, *A.J.*, **83**, 162.
Ciardullo, R. B., and Demarque, P. 1977, *Yale Trans.*, **33**.
Clegg, R. E. S., Lambert, D. L., and Tomkin, J. 1981, *Ap. J.*, **250**, 262.
Cohen, R. S., Thaddeus, P., and Bronfman, L. 1984, in *IAU Symposium 106, The Milky Way Galaxy*, ed. H. van Woerden, W. B. Burton, and K. J. Allen (Dordrecht: Reidel), in press.
Cox, D. P., and Smith, B. W. 1976, *Ap. J.*, **203**, 361.
Crovisier, J. 1978, *Astr. Ap.*, **70**, 43.
de Vaucouleurs, G., and Pence, W. D. 1978, *A.J.*, **83**, 1163.
Dickman, R. L. 1978, *Ap. J. Suppl.*, **37**, 407.
Fall, S. M., and Efstathiou, G. 1980, *M.N.R.A.S.*, **193**, 189.
Fich, M., and Blitz, L. 1984, *Ap. J.*, **279**, 125.
Frerking, M. A., Langer, W. D., and Wilson, R. W. 1982, *Ap. J.*, **262**, 590.
Fukunaga, M. 1983, *Pub. Astr. Soc. Japan*, **35**, 173.
Garmany, C. D., Conti, P. S., and Chiosi, C. 1982, *Ap. J.*, **263**, 777.
Goldreich, P., and Lynden-Bell, D. 1965, *M.N.R.A.S.*, **130**, 125.
Goldreich, P., and Tremaine, S. 1978, *Icarus*, **34**, 227.
Güsten, R., and Mezger, M. 1982, *Vistas Astr.*, **26**, 159.
Guibert, J., Lequeux, J., and Viallefond, F. 1978, *Astr. Ap.*, **68**, 1.
Hamajima, K., and Tosa, M. 1975, *Pub. Astr. Soc. Japan*, **27**, 561.
Harris, H. C. 1981, *A.J.*, **86**, 707.
Hawley, S. A. 1978, *Ap. J.*, **224**, 417.
Heiles, C. 1976, *Ap. J.*, **204**, 379.
Henderson, A. P., Jackson, P. D., and Kerr, F. J. 1982, *Ap. J.*, **263**, 116.
Hermsen, W., and Bloemen, J. B. G. M. 1984, in *IAU Symposium 106, The Milky Way Galaxy*, ed. H. van Woerden, W. B. Burton, and K. J. Allen (Dordrecht: Reidel), in press.
Humphreys, R. M., and McElroy, D. B. 1984, *Ap. J.*, **284**, 565.
Janes, K. A. 1979, *Ap. J. Suppl.*, **39**, 135.

Janes, K., and Demarque, P. 1983, *Ap. J.*, **264**, 206.
Kalnajs, A. J. 1972, *Ap. Letters*, **11**, 41.
Kennicutt, R. C. 1983, *Ap. J.*, **272**, 54.
Kerr, F. J. 1962, *M.N.R.A.S.*, **123**, 327.
———. 1969, *Ann. Rev. Astr. Ap.*, **7**, 39.
Kormendy, J. 1977, *Ap. J.*, **217**, 406.
Kulkarni, S. R., Blitz, L., and Heiles, C. 1982, *Ap. J. (Letters)*, **259**, L63 (KBH).
Lacey, C. G. 1984, Ph.D. thesis, University of Cambridge.
Lacey, C. G., and Fall, S. M. 1983, *M.N.R.A.S.*, **204**, 791 (Paper I).
Larson, R. B. 1972, *Nature Phys. Sci.*, **236**, 7.
Larson, R. B., Tinsley, B. M., and Caldwell, C. N. 1980, *Ap. J.*, **237**, 692.
Lebrun, F., *et al.* 1983, *Ap. J.*, **274**, 231.
Lynden-Bell, D. 1975, *Vistas Astr.*, **19**, 299.
Lynden-Bell, D., and Pringle, J. E. 1974, *M.N.R.A.S.*, **168**, 603.
Lyne, A. G., Manchester, R. N., and Taylor, J. H. 1984, in preparation.
Maeder, A. 1981, *Astr. Ap.*, **101**, 385.
Mayor, M., and Vigroux, L. 1981, *Astr. Ap.*, **98**, 1.
Mezger, P. G. 1978, *Astr. Ap.*, **70**, 565.
Miller, G. E., and Scalo, J. M. 1979, *Ap. J. Suppl.*, **41**, 513.
Mirabel, I. F., and Morras, R. 1984, *Ap. J.*, **279**, 86.
Oort, J. H. 1970, *Astr. Ap.*, **7**, 381.
———. 1977, *Ann. Rev. Astr. Ap.*, **15**, 295.
Pagel, B. E. J., and Edmunds, M. G. 1981, *Ann. Rev. Astr. Ap.*, **19**, 77.
Pagel, B. E. J., and Patchett, B. E. 1975, *M.N.R.A.S.*, **172**, 13.
Peimbert, M., Torres-Peimbert, S., and Rayo, J. F. 1978, *Ap. J.*, **220**, 516.
Potter, D. 1973, *Computational Physics* (London: Wiley).
Quirk, W. J., and Tinsley, B. M. 1973, *Ap. J.*, **179**, 69.
Radhakrishnan, V., and Sarma, N. V. G. 1980, *Astr. Ap.*, **85**, 249.
Roberts, W. W. 1969, *Ap. J.*, **158**, 123.
Roberts, W. W., and Shu, F. H. 1972, *Ap. Letters*, **12**, 49.
Sancisi, R. 1983, in *IAU Symposium 100, Internal Kinematics and Dynamics of Galaxies*, ed. E. Athanassoula (Dordrecht: Reidel), p. 55.
Sanders, D. B., Solomon, P. M., and Scoville, N. Z. 1984, *Ap. J.*, **276**, 182.
Schmidt, M. 1959, *Ap. J.*, **129**, 243.
———. 1963, *Ap. J.*, **137**, 758.
Schwarz, M. P. 1981, *Ap. J.*, **247**, 77.
Shaver, P. A., McGee, R. X., Newton, L. M., Danks, A. C., and Pottasch, S. R. 1983, *M.N.R.A.S.*, **204**, 53.
Shu, F. H., Milione, V., and Roberts, W. W. 1973, *Ap. J.*, **183**, 819.
Stark, A. A. 1984, *Ap. J.*, **281**, 624.
Talent, D. L., and Dufour, R. J. 1979, *Ap. J.*, **233**, 888.
Thaddeus, P. 1983, private communication.

LACEY AND FALL

Tinsley, B. M. 1980, *Fund. Cosmic Phys.*, **5**, 287.
Tinsley, B. M., and Larson, R. B. 1978, *Ap. J.*, **221**, 554.
Twarog, B. A. 1980, *Ap. J.*, **242**, 242.
Twarog, B. A., and Wheeler, J. C. 1982, *Ap. J.*, **261**, 636.
van Albada, G. D., and Roberts, W. W. 1981, *Ap. J.*, **246**, 741.
Vandenberg, D. A. 1983, *Ap. J. Suppl.*, **51**, 29.
van der Kruit, P. C. 1983, *Publ. Astr. Soc. Australia*, **5**, 136.

van der Kruit, P. C., and Searle, L. 1982, *Astr. Ap.*, **110**, 61.
Velden, L. 1970, *Beiträge zur Radioastronomie* (Max-Planck-Institut für Radioastronomie, Bonn), **1**, 221.
Webster, B. L., and Smith, M. G. 1983, *M.N.R.A.S.*, **204**, 743.
Wielen, R. 1979, in *IAU Symposium 84, The Large-Scale Characteristics of the Galaxy*, ed. W. B. Burton (Dordrecht: Reidel), p. 133.

S. MICHAEL FALL: Space Telescope Science Institute, Homewood Campus, Baltimore, MD 21218

CEDRIC G. LACEY: Princeton University Observatory, Peyton Hall, Princeton, NJ 08544